Supplementary tables

Table S1. The enrolled pan-cancer scRNA-seq cohorts in this study.

No	Dataset	Cancer	Patients	Cells	Platform	PMID
1	GSE123813	BCC	11	52884	10x Genomics	31359002
2	GSE141526	BCC	6	56116	10x Genomics	33033234
3	GSE149652	BLCA	28	30604	Illumina	32497499
4	EMTAB8107	BRCA	14	33043	10x Genomics	32561858
5	GSE148673	BRCA	6	10359	10x Genomics	33462507
6	GSE176078	BRCA	26	89471	10x Genomics	34493872
7	EMTAB8107	CRC	7	23176	10x Genomics	32561858
8	GSE146771	CRC	10	10468	Smart-seq2	32302573
9	GSE179784	CRC	4	12118	DNBSEQ-G50	36443332
10	GSE139448	GBM	3	12152	10x Genomics	32004492
11	GSE141982	GBM	2	5263	10x Genomics	32105316
12	GSE103322	HNSC	18	5902	Smart-seq2	29198524
13	GSE125449	LIHC	9	3834	10x Genomics	31588021
14	GSE119926	MB	25	7745	Smart-seq2	31341285
15	GSE117988	MCC	1	10134	10x Genomics	30250229
16	GSE118056	MCC	1	11024	10x Genomics	30250229
17	GSE117156	MM	14	24918	MARS-seq	30523328
18	EMTAB6149	NSCLC	8	40218	10x Genomics	29988129
19	GSE117570	NSCLC	4	11453	10x Genomics	31033233
20	GSE127465	NSCLC	7	31179	Smart-seq2	30979687
21	GSE150660	NSCLC	2	5407	10x Genomics	32675368
22	GSE118828	OV	9	1909	Smart-seq2	30383866
23	CRA001160	PAAD	35	57443	10x Genomics	31273297
24	GSE111672	PAAD	3	6122	inDrop	31932730
25	GSE115978	SKCM	31	7186	Smart-seq2	30388455
26	GSE72056	SKCM	19	4645	Smart-seq2	27124452
27	GSE134520	STAD	13	41554	10x Genomics	31067475
28	GSE139829	UVM	11	103703	10x Genomics	31980621
	Overall		327	710030		

Table S2. The small interfering RNA sequences.

Gene	Sequence(5'-3')
NC-RNAi-1	UUCUCCGAACGUGUCACGU
	ACGUGACACGUUCGGAGAA
FCHO1-RNAi-1	GGAAGUUUGCAGAGAGUAAGG
	UUACUCUCUGCAAACUUCCUG
FCHO1-RNAi-2	AGUUCUAUGUGCACAUCAAGC
	UUGAUGUGCACAUAGAACUUG
Nc-RNAi-1	GCGCGCUUUGUAGGAUUCG
	CGAAUCCUACAAAGCGCGC
Fcho1-RNAi-1	AGUUCUAUGUUCACAUCAAGC
	UUGAUGUGAACAUAGAACUUU
Fcho1-RNAi-2	GGAAAUUUGCAGAGAGCAAGG
	UUGCUCUCUGCAAAUUUCCUG

Table S3. The antibodies used in this study.

Antibodies	Source	Cat No.	Application
FCHO1	Proteintech	26767-1-AP	WB
Fcho1	Affinity	DF13832	WB
GAPDH	Proteintech	60004-1-Ig	WB
OXPHOS Cocktail	Proteintech	PK30006	WB
ZAP70	Proteintech	15592-1-AP	WB
Phospho-*ZAP70* (Tyr319)/SYK (Tyr352)	Proteintech	81767-2-RR	WB
p70(S6K)	Proteintech	14485-1-AP	WB
Phospho-p70(S6K) (Thr389)/p85(S6K) (Thr412)	Proteintech	28735-1-AP	WB
4EBP1	Proteintech	60246-1-Ig	WB
Phospho-*4EBP1* (Thr37)	Proteintech	81812-4-RR	WB
mTOR	Proteintech	20657-1-AP	WB
Phospho-*mTOR* (Ser2448)	Proteintech	67778-1-Ig	WB
ERK1/2	Proteintech	11257-1-AP	WB
Phospho-ERK1/2 (Thr202/Tyr204)	Proteintech	28733-1-AP	WB
Beta Actin	Proteintech	66009-1-Ig	WB
CFSE	Selleck	S8269	FCM
Zombie Aqua™ Fixable Viability Kit	Biolegend	423101	FCM
CD45	BD Horizon™	564105	FCM
CD3	BD Horizon™	562426	FCM
CD4	BD Horizon™	566318	FCM
CD8	BD Horizon™	563823	FCM
CD25	BD Horizon™	560989	FCM
CD69	BD Horizon™	560967	FCM
TIM-3	BD Horizon™	563422	FCM
CTLA-4	BD Horizon™	560938	FCM
PD-1	BD Horizon™	560908	FCM
LAG-3	BD Horizon™	565716	FCM
Cd45	Biolegend	103116	FCM
Cd3	Biolegend	100216	FCM
Cd8	Biolegend	100744	FCM
Gzmb	Biolegend	396414	FCM
Ifn-γ	Biolegend	505838	FCM
Tnf-α	Biolegend	506306	FCM
Pd-1	Biolegend	135213	FCM
Cyto-Fast™ Fix/Perm Buffer Set	Biolegend	426803	FCM
Cd8	Proteintech	29896-1-AP	IHC
Tnf-α	Proteintech	17590-1-AP	IHC
Gzmb	Proteintech	13588-1-AP	IHC
Pd-1	Proteintech	66220-1-Ig	IHC

Antibodies	Source	Cat No.	Application
Tigit	Proteintech	83545-1-RR	IHC
FCHO1	Abcam	ab272640	IHC; IF
PanCK	AiFang	AF20164	IF
CD8	AiFang	AF20211	IF
PD-L1	AiFang	AF20084	IF
CD20	AiFang	AFRM0016	IF
CD68	AiFang	AFRM0021	IF
CD3	AiFang	AFRM0030	IF
CD3	Proteintech	60181-1-Ig	IF
Clathrin	Proteintech	26523-1-AP	IF
IFN-γ	MSKBIO	KT90110	ELISA
TNF-α	MSKBIO	KT-99985	ELISA
GZMB	Invitrogen	BMS6029	ELISA

Table S4. Primer sequences used for qPCR.

Gene	Sequence(5'-3')
FCHO1-Forward (qPCR)	GCGAGAACTACCTGAACCGTTGC
FCHO1-Reverse (qPCR)	TCTCCGCCTTGTCCATCTCCTTC
Fcho1-Forward (qPCR)	CCACTGTCCAAGAGCCTCTTTG
Fcho1-Reverse (qPCR)	AAAGGAGACGGGCTGGATGTGA
GAPDH-Forward (qPCR)	GTCTCCTCTGACTTCAACAGCG
GAPDH-Reverse (qPCR)	ACCACCCTGTTGCTGTAGCCAA
Gapdh-Forward (qPCR)	CATCACTGCCACCCAGAAGACTG
Gapdh-Reverse (qPCR)	ATGCCAGTGAGCTTCCCGTTCAG

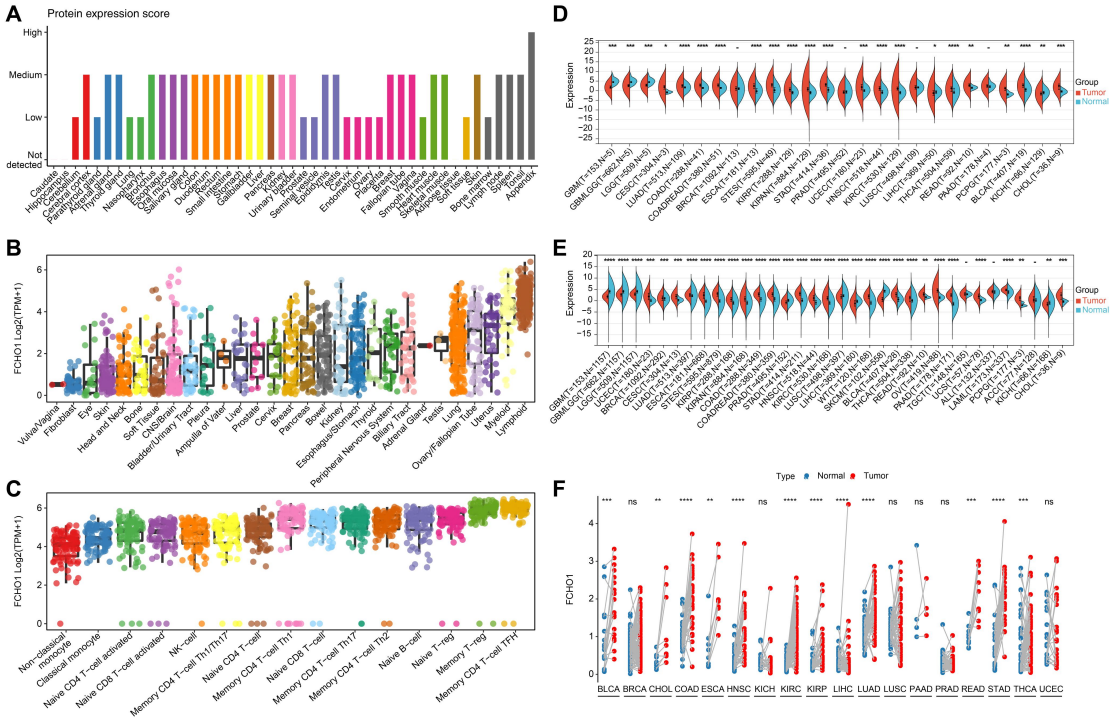


Figure S1. Differential expression analysis of *FCHO1* across normal tissues, cancer cell lines, immune cell types, and pan-cancer datasets. (A) Protein expression score of *FCHO1* across human normal tissues based on data from the Human Protein Atlas (HPA) database. **(B)** *FCHO1* mRNA expression profile across pan-cancer cell lines from the Cancer Cell Line Encyclopedia (CCLE) expression dataset. **(C)** *FCHO1* mRNA expression profile across various immune cell types from the DICE expression database. **(D)** *FCHO1* expression across pan-cancer types based on the TCGA dataset. Blue represents normal tissues and red represents tumor tissues. **(E)** *FCHO1* expression across pan-cancer types based on combined TCGA and GTEx datasets. Blue represents normal tissues and red represents tumor tissues. **(F)** *FCHO1* expression in paired tumor and adjacent normal samples across selected cancer types from the TCGA database. *p < 0.05; **p < 0.01; ***p < 0.001; ****p < 0.0001; ns, not significant.

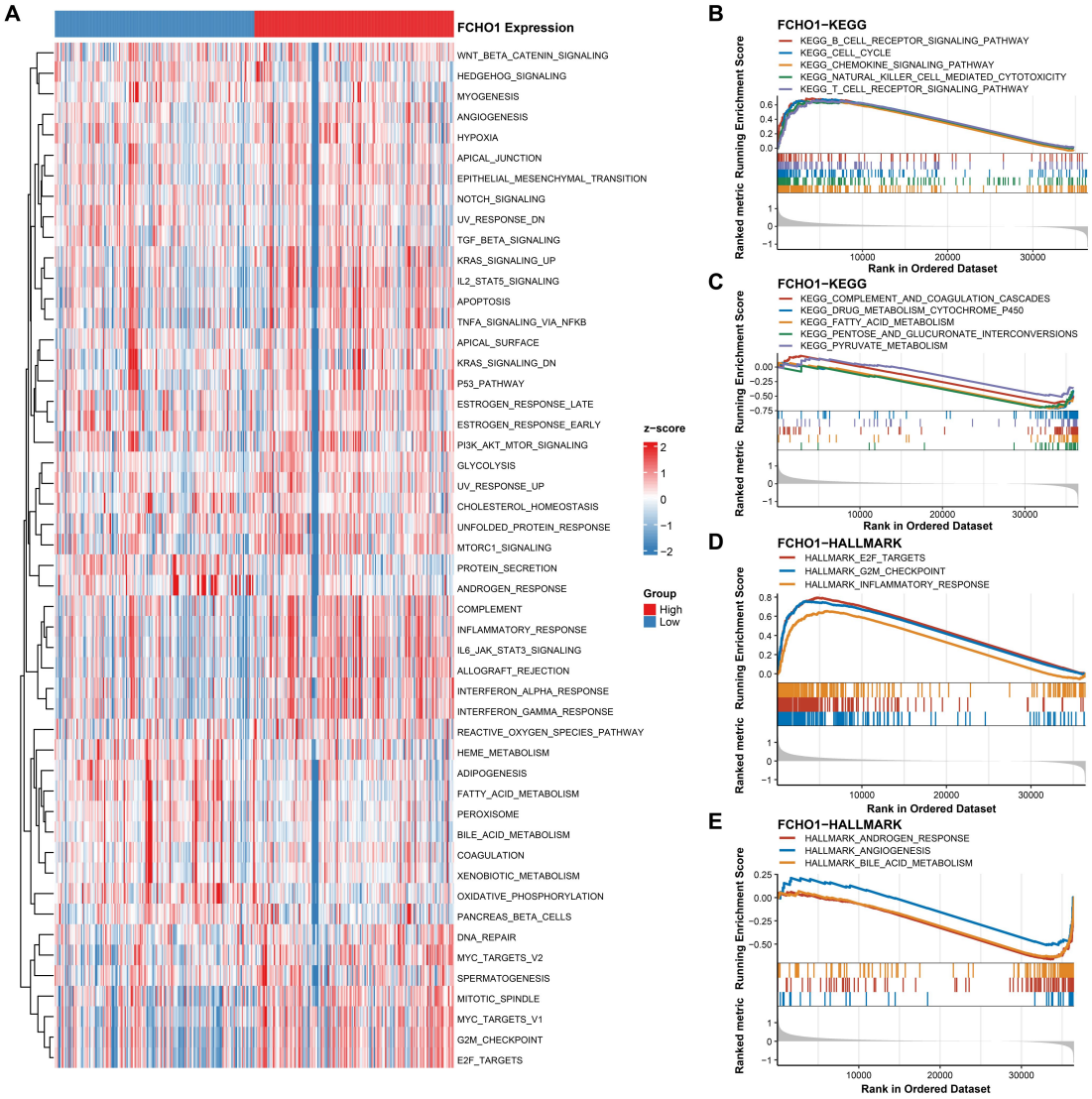


Figure S2. Functional Enrichment Analysis Based on *FCHO1* Expression in the TCGA Pan-Cancer Dataset. According to the median expression value of *FCHO1* in the TCGA pan-cancer dataset, patients were classified into high and low expression groups. Functional enrichment analysis was conducted using the GSVA algorithm. **(A)** Heatmap illustrating the enrichment of significant hallmark gene sets. **(B)** Five positively enriched pathways and **(C)** five negatively enriched pathways based on KEGG terms. **(D)** Three positively enriched pathways and **(E)** three negatively enriched pathways based on Hallmark terms.

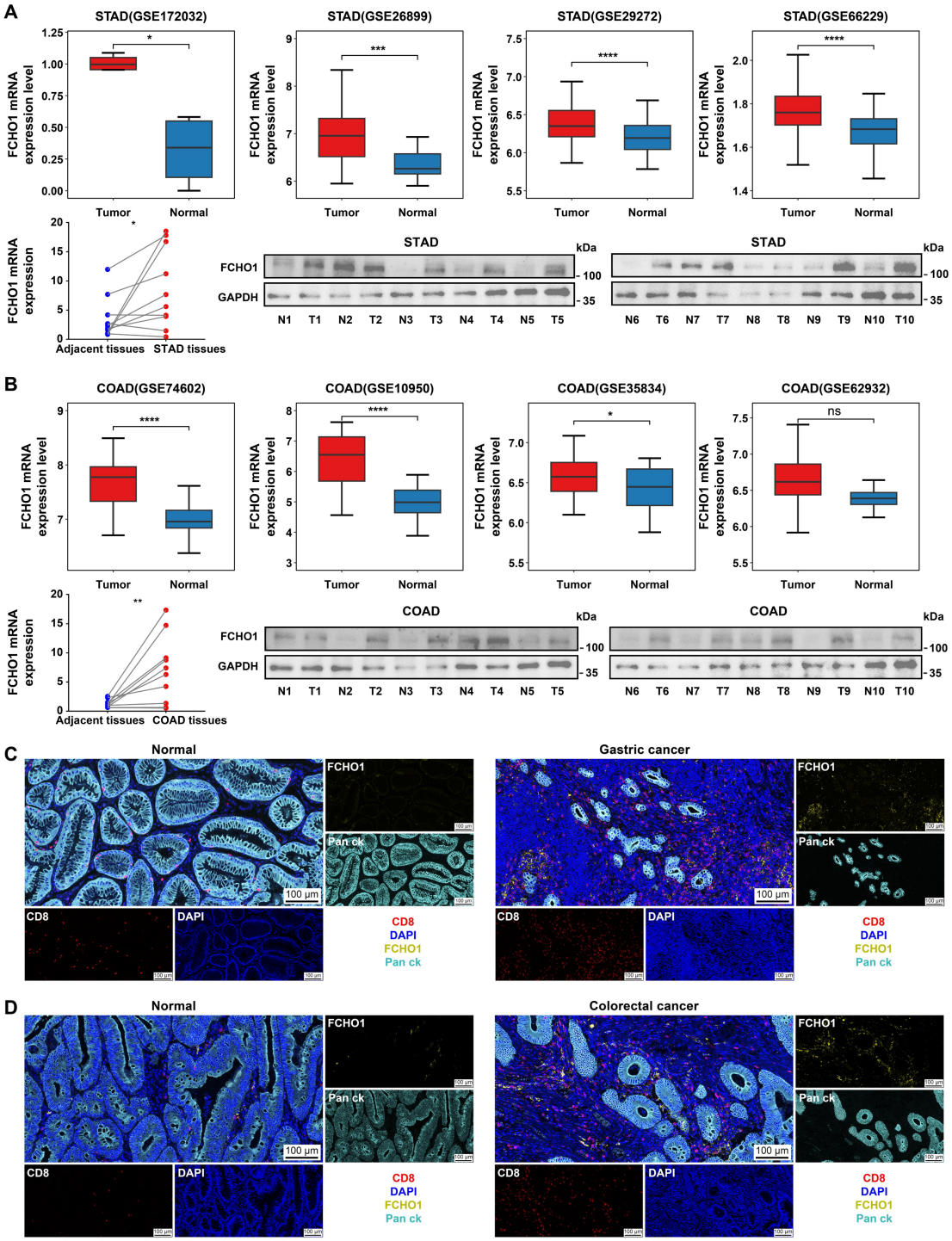


Figure S3. *FCHO1* expression in gastric cancer and colorectal cancer datasets and tissue validation. (A) *FCHO1* mRNA expression differences in gastric cancer (STAD) across four GEO datasets (GSE172032, GSE26899, GSE29272, GSE66229), with paired dot plots showing *FCHO1* mRNA levels in 10 paired gastric cancer (STAD) and adjacent normal tissues, and Western blot analysis of *FCHO1* protein levels in the same paired samples (N: adjacent normal tissue; T: tumor tissue). **(B)** *FCHO1* mRNA expression differences in colorectal cancer (COAD) across four GEO datasets (GSE74602, GSE10950, GSE35834, GSE62932), with paired dot plots showing *FCHO1* mRNA levels in 10 paired colorectal cancer (COAD) and adjacent normal tissues, and Western blot analysis of *FCHO1* protein levels in the same paired

samples (N: adjacent normal tissue; T: tumor tissue). **(C)** Representative multiplex immunofluorescence images showing *FCHO1* (yellow), CD8 (red), Pan-CK (cyan), and DAPI (blue) staining in normal gastric tissue and gastric cancer tissue. Scale bar, 100 μm. **(D)** Representative multiplex immunofluorescence images showing *FCHO1* (yellow), CD8 (red), Pan-CK (cyan), and DAPI (blue) staining in normal colorectal tissue and colorectal cancer tissue. Scale bar, 100 μm. *p < 0.05; **p < 0.01; ***p < 0.001; ****p < 0.0001; ns: not significant.

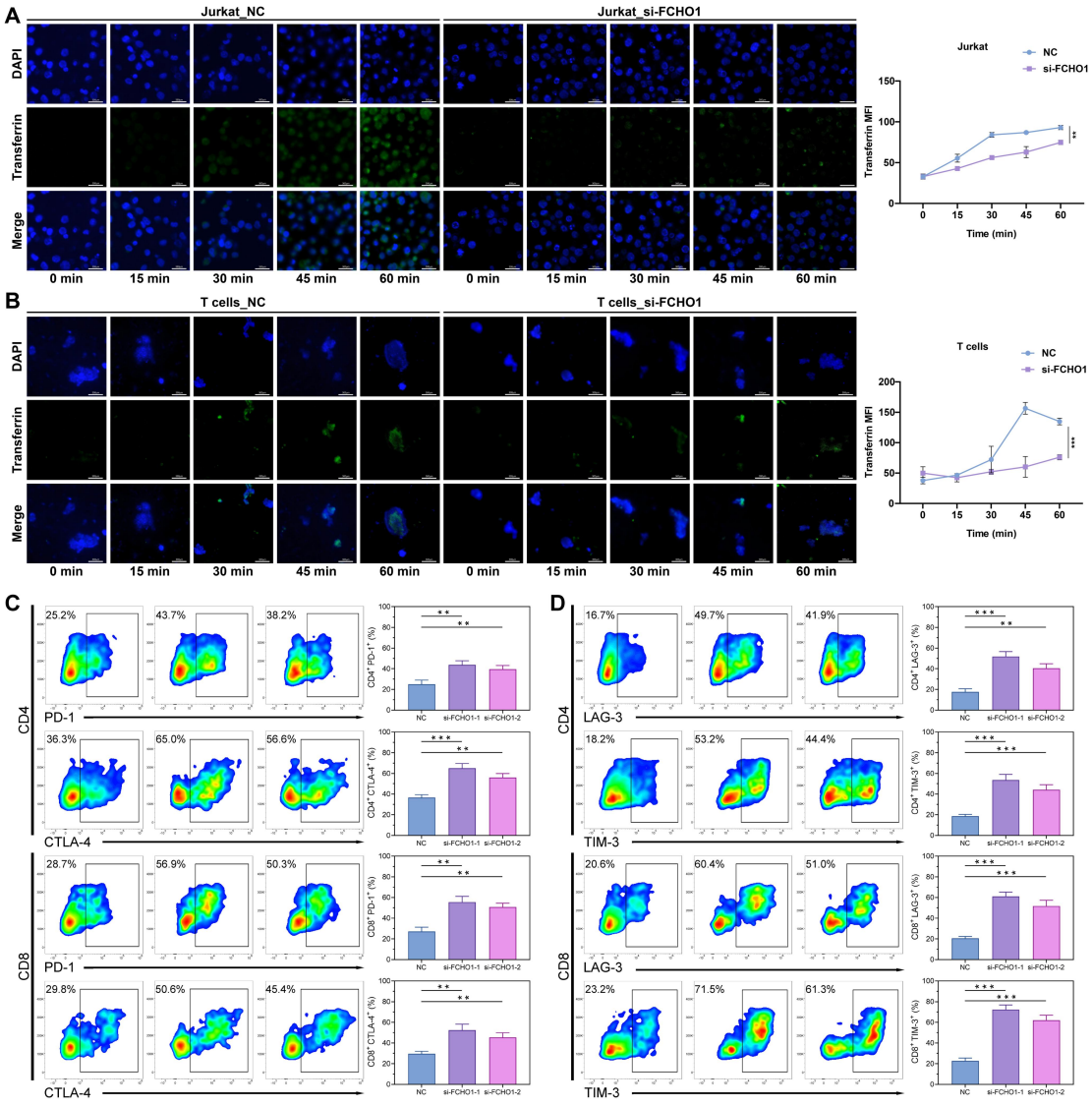


Figure S4. *FCHO1* regulates T-cell immune phenotype by clathrin-mediated endocytosis (CME). (A) Immunofluorescence indicates that *FCHO1* knockdown impairs transferrin uptake in Jurkat cells. **(B)** Immunofluorescence indicates that *FCHO1* knockdown impairs transferrin uptake in T cells. Scale bar, 300 μm. **(C)** *FCHO1* knockdown affects exhaustion markers (*PD-1*, *CTLA-4*) in CD4+ and CD8+ T cells. **(D)** *FCHO1* knockdown alters the exhaustion markers, *LAG-3* and *TIM-3*, in CD4+ and CD8+ T cells. Data are presented as mean ± s.d. from n = 3 biologically independent experiments. **p < 0.01; ***p < 0.001.

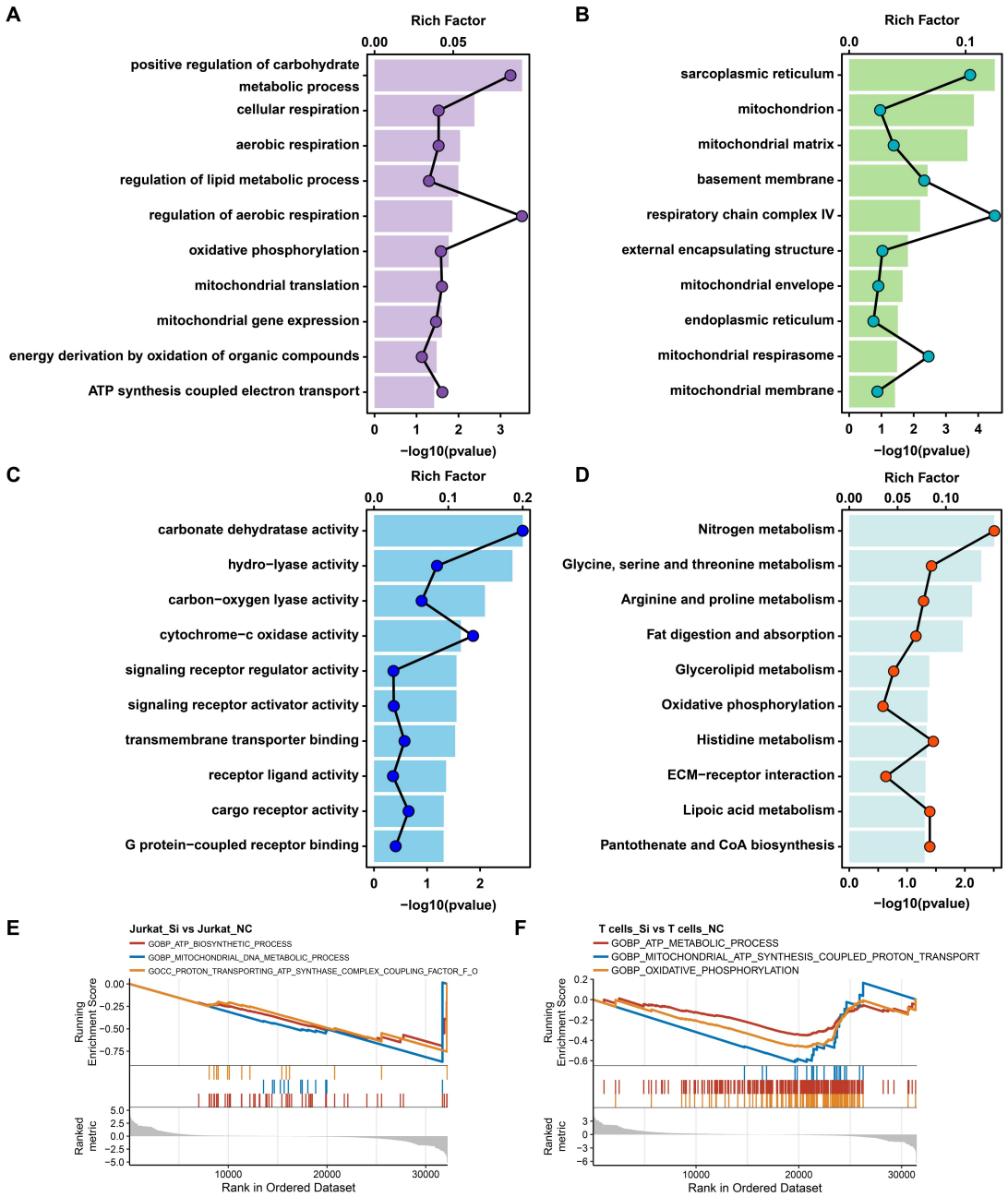


Figure S5. Bioinformatics analysis indicated pathways significantly downregulated after *FCHO1* knockdown in Jurkat cells and T cells. (A) GO analysis of Biological Processes (BP). **(B)** GO analysis of Cellular Components (CC). **(C)** GO analysis of Molecular Functions (MF). **(D)** KEGG pathway analysis. **(E-F)** GSEA indicated significantly downregulated pathways after *FCHO1* knockdown. RNA-seq was performed with n = 3 biological replicates per group.

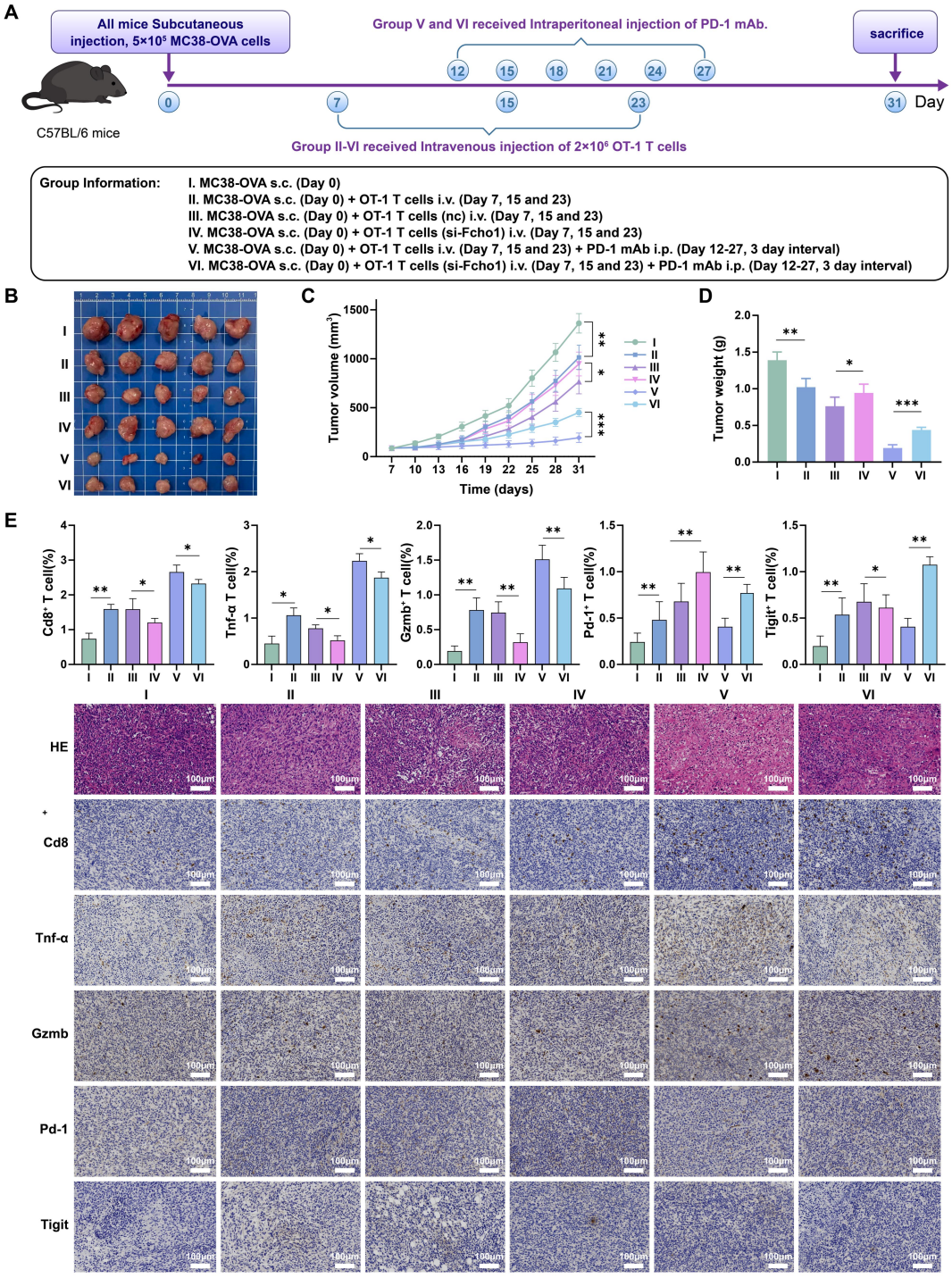


Figure S6. The effect of *Fcho1*-knockdown T cells on syngeneic tumor growth and immunotherapy efficacy. (A) Schematic of the syngeneic tumor immunotherapy treatment protocol, evaluating the effect of *Fcho1* knockdown in OT-1 CD8+ T cells on syngeneic tumor immunotherapy. **(B)** Representative images of subcutaneous MC38-OVA tumor syngeneic tumor for each experimental group (n = 5 per group). **(C)** Tumor growth curves for each experimental group. **(D)** Comparison of tumor weights at the endpoint for each experimental group. **(E)** Representative H&E

staining, IHC staining, and statistical results for immune markers (Cd8, *Tnf-α*, *Gzmb*, *Pd-1*, Tigit) at the endpoint. Scale bar, 100 μm. Data are presented as mean ± s.e.m.*p < 0.05; **p < 0.01; ***p < 0.001; ns, not significant.

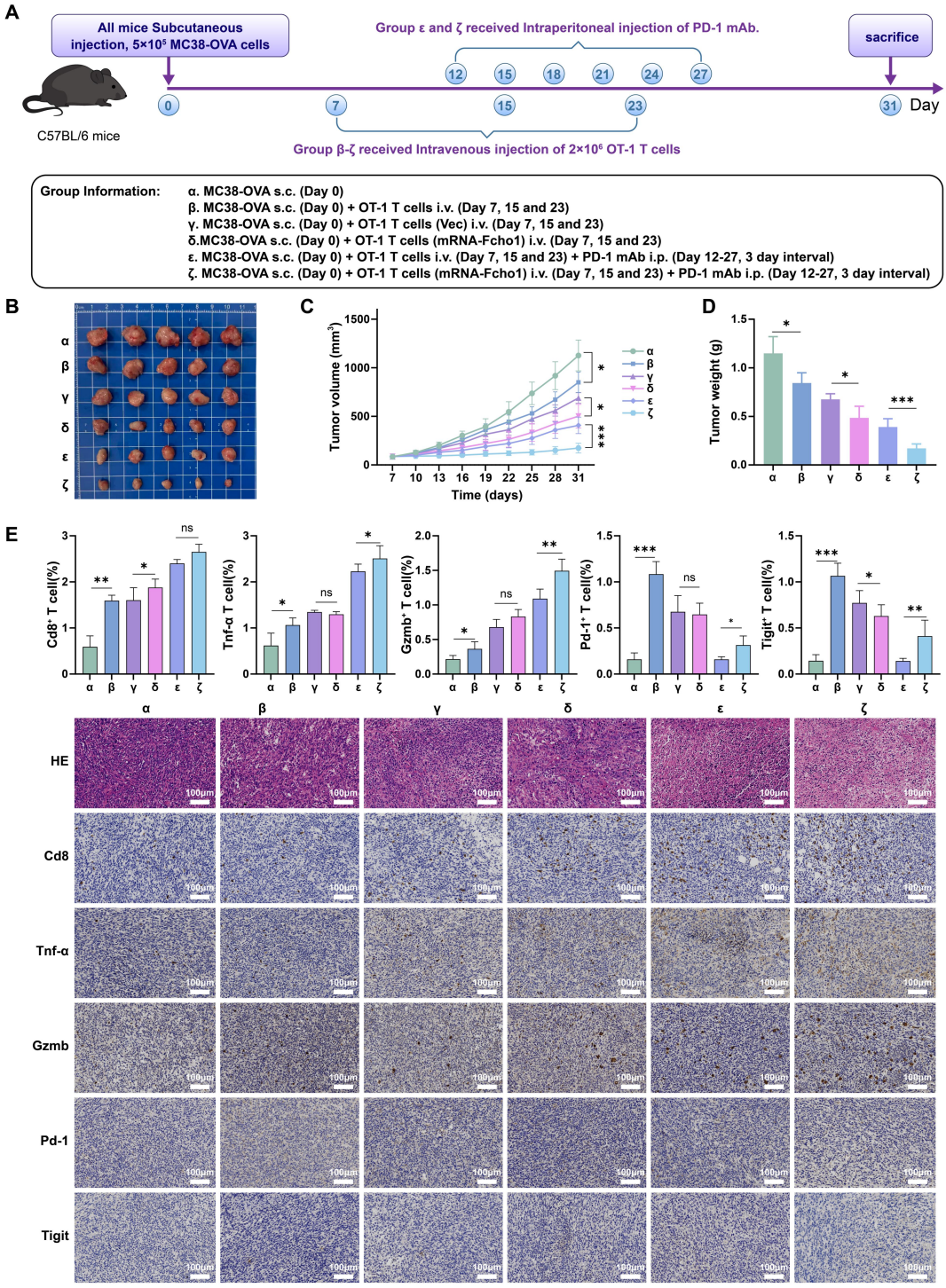


Figure S7. The effect of *Fcho1*-modulated T cells on syngeneic tumor growth and immunotherapy efficacy. (A) Schematic of the syngeneic tumor immunotherapy treatment protocol, evaluating the effect of *Fcho1* overexpression in OT-1 CD8+ T cells on syngeneic tumor immunotherapy. **(B)** Representative images of subcutaneous MC38-OVA tumor syngeneic tumor for each experimental group (n = 5 per group). **(C)** Tumor growth curves for each experimental group. **(D)** Comparison of tumor

weights at the endpoint for each experimental group. **(E)** Representative H&E staining, IHC staining, and statistical results for immune markers (Cd8, *Tnf-α*, *Gzmb*, *Pd-1*, Tigit) at the endpoint. Scale bar, 100 μm. Data are presented as mean ± s.e.m. *p < 0.05; **p < 0.01; ***p < 0.001; ns, not significant.

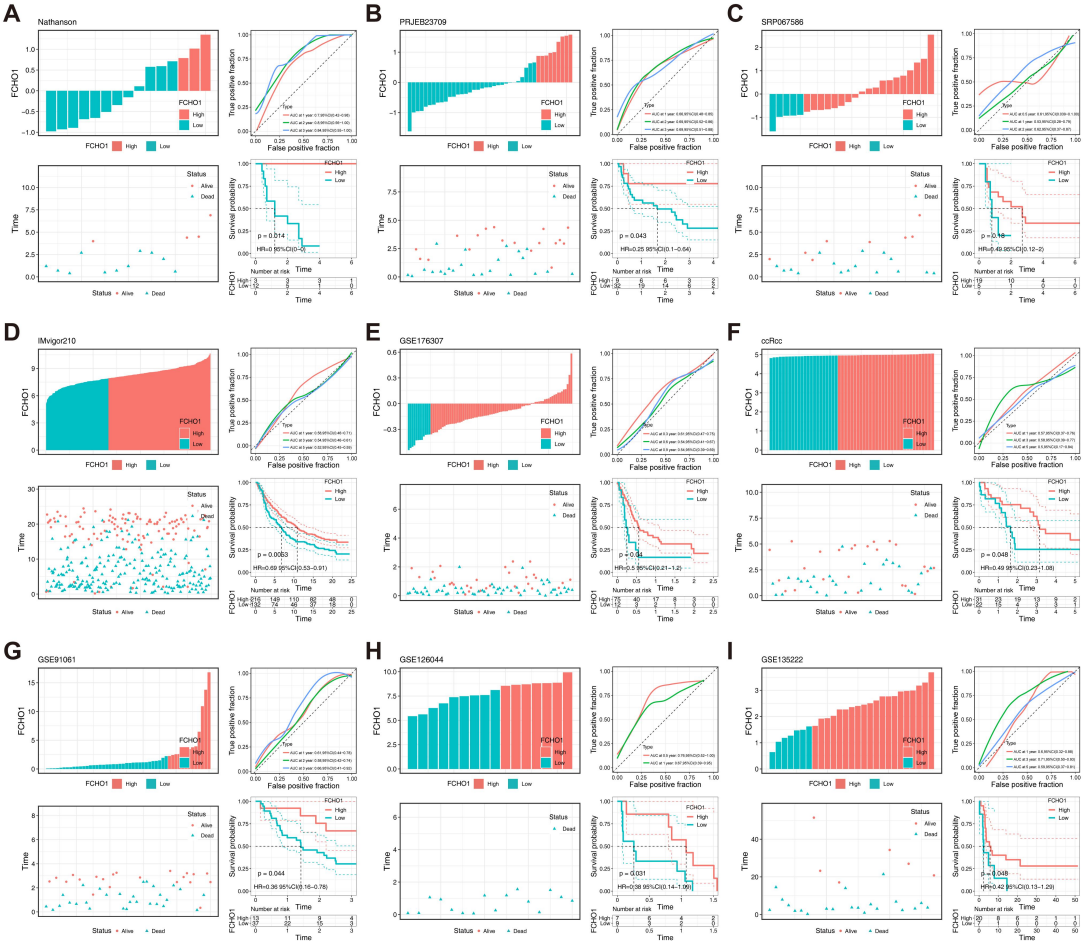


Figure S8. Multiple immunotherapy cohorts indicate that high expression of *FCHO1* was significantly correlated with an increased response to immunotherapy. (A-C) The prognostic difference and predictive value of high/low expression of *FCHO1* in various melanoma immunotherapy cohorts. **(D-F)** The prognostic difference and predictive value of high/low expression of *FCHO1* in different urothelial cancer immunotherapy cohorts. **(G-I)** The prognostic difference and predictive value of high/low expression of *FCHO1* in different NSCLC immunotherapy cohorts.

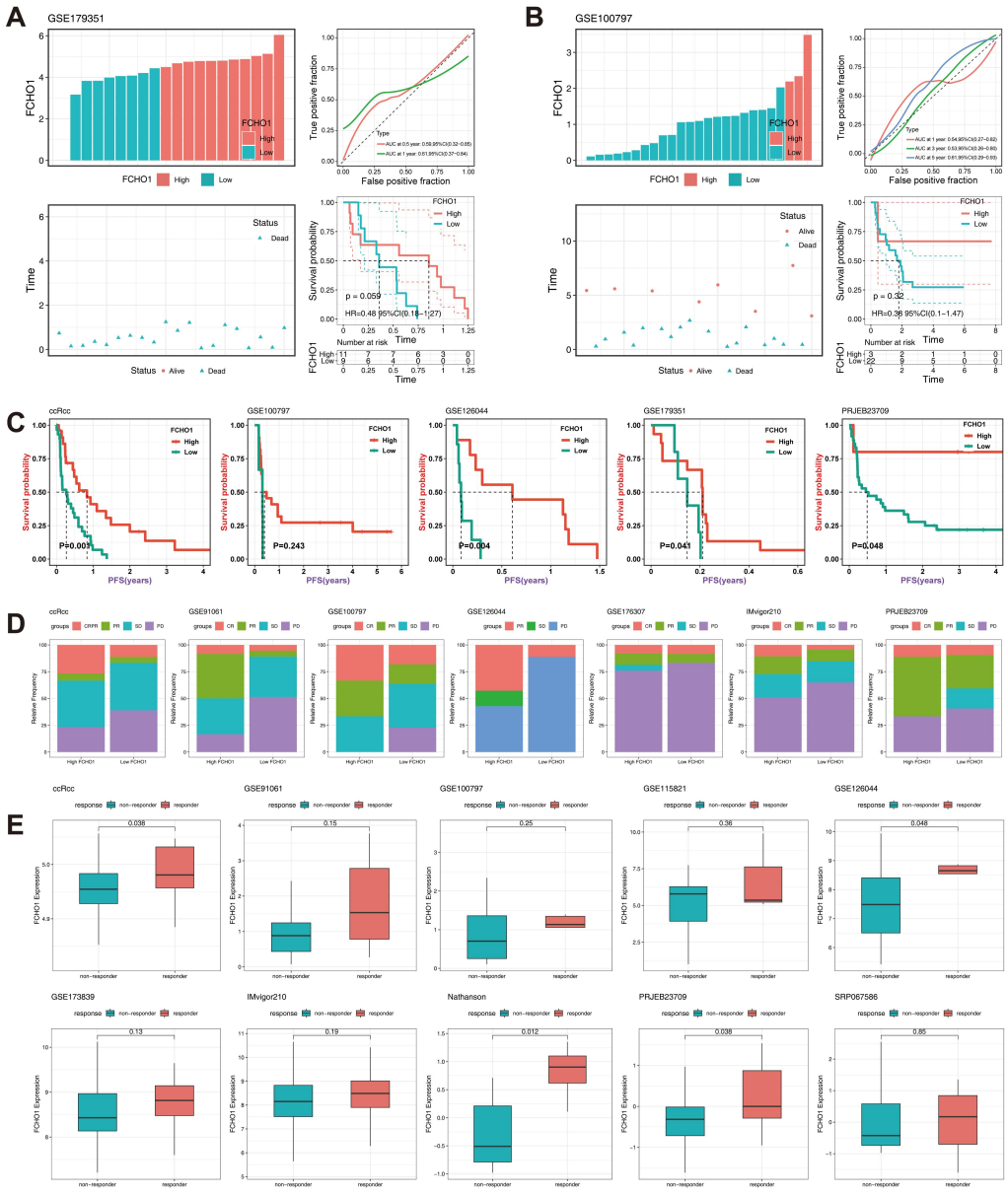


Figure S9. High and low expression of *FCHO1* in multiple immunotherapy cohorts suggests different OS and PFS, and different immunotherapy responses in patients. (A-B) The prognostic differences and predictive value of high and low expression of *FCHO1* in COAD, PAAD, and adoptive T cell therapy (ACT) immunotherapy cohorts. **(C)** High and low expression of *FCHO1* in multiple immunotherapy cohorts suggests different PFS. **(D-E)** High and low expression of *FCHO1* in multiple immunotherapy cohorts suggests different immunotherapy responses in patients.

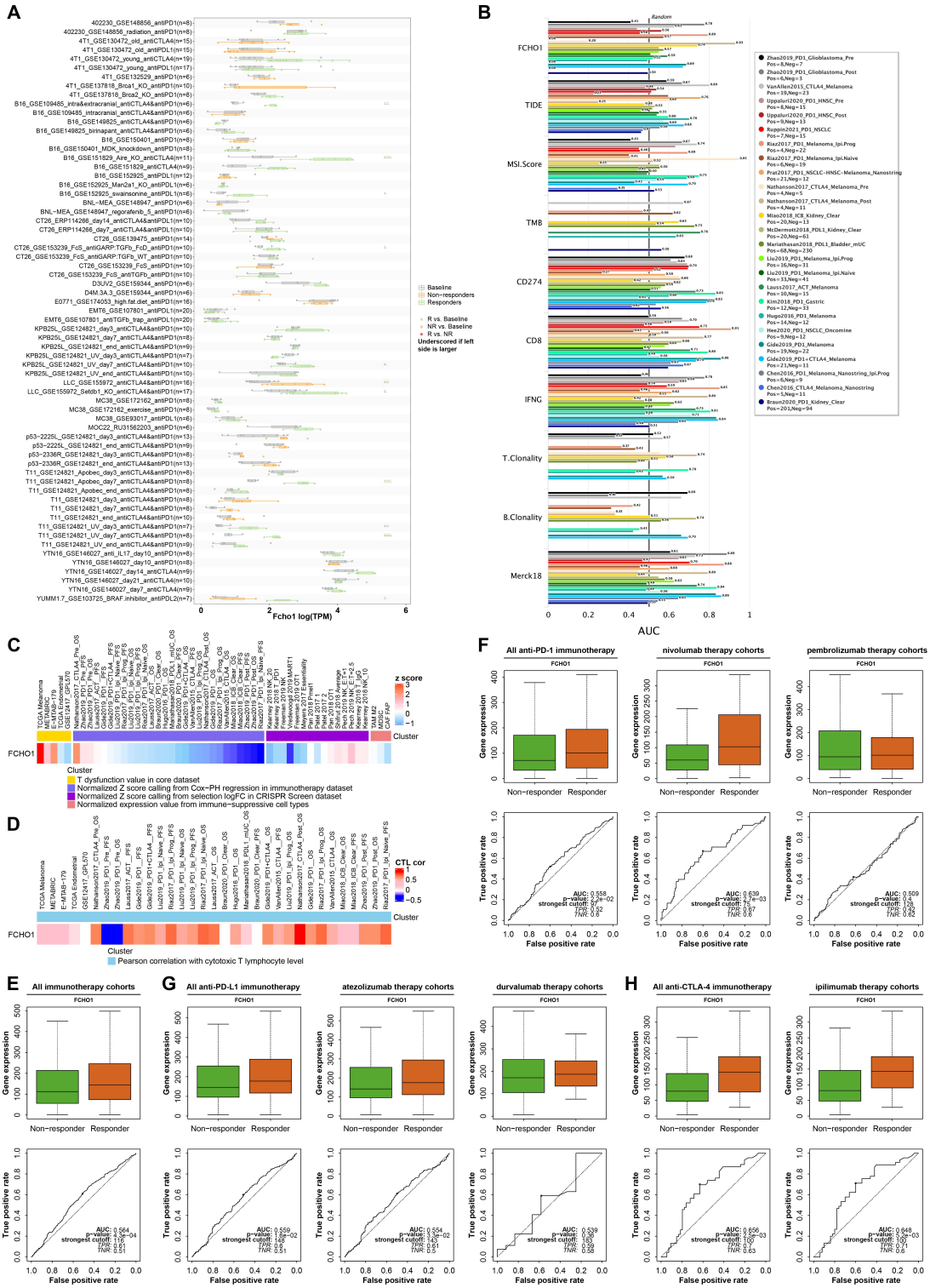


Figure S10. Immunotherapy response and biomarker relevance prediction of *FCHO1* in pan-cancer. Immunotherapy response **(A)** and biomarker relevance **(B)** of *FCHO1* in immunotherapy cohorts based on TISMO and TIDE online database. **(C-D)** The heatmap indicated a significant correlation of *FCHO1* with several indicators of immunosuppression/immunostimulation in different immunotherapy cohorts of the TIDE dataset. Box plots show the *FCHO1* expression differences between responders and non-responders in different immunotherapy cohorts, and the ROC presents the predictive accuracy of the patient therapeutic response by *FCHO1* levels on the ROC

Plotter online website. **(E)** All immunotherapy cohorts, **(F)** All anti-*PD-1* immunotherapy, nivolumab, and pembrolizumab therapy cohorts. **(G)** All anti-*PD-L1* immunotherapy, atezolizumab, and durvalumab therapy cohorts. **(H)** All anti-*CTLA-4* immunotherapy and ipilimumab therapy cohorts.